Acta Crystallographica Section A
Foundations of Crystallography
ISSN 0108-7673

Received 29 June 2012
Accepted 20 February 2013

Anisotropic displacement parameters for molecular crystals from periodic Hartree–Fock and density functional theory calculations

Anders Østergaard Madsen,[a]* Bartolomeo Civalleri,[b] Matteo Ferrabone,[b] Fabien Pascale[c] and Alessandro Erba[b]

[a]Department of Chemistry, University of Copenhagen, Denmark, [b]Department of Chemistry and NIS Centre of Excellence, University of Torino, Italy, and [c]5Q, rue du Beaujolais, 54500 Vandoeuvre-lès-Nancy Cedex 05, France. Correspondence e-mail: madsen@chem.ku.dk

Fully periodic Hartree–Fock and density functional theory calculations have been used to compute the anisotropic displacement parameters (ADPs) of molecular crystals at different temperatures by using the *CRYSTAL* code. Crystalline urea was adopted as a benchmark system to investigate the dependence on basis set and Hamiltonian. The results were compared with ADPs derived from neutron diffraction experiments. The approach can estimate the internal ADPs, corresponding to the contributions of high-frequency intramolecular vibrations, and for these internal contributions the results are almost independent of the basis set and Hamiltonian. Much larger variations and discrepancies from neutron diffraction experiments are seen for the external, low-frequency modes, which become dominant at higher temperatures. The approach was then tested on benzene and urotropine. Finally, ADPs of L-alanine were predicted at the B3LYP/6-31G(d,p) level of theory. The total ADPs, including low-frequency external modes, are underestimated, but can be brought into good agreement with the experimental ADPs by introducing a Grüneisen parameter, which partly accounts for anharmonicity of the potential energy surface, but likely also contains contributions from other deficiencies of the calculations.

1. Introduction

The physical significance of anisotropic displacement parameters (ADPs) derived from X-ray and neutron diffraction experiments, as reflecting the mean-square atomic displacements, has been discussed for many years. Uncorrected systematic errors like absorption and scan truncation effects as well as deviations from the kinematic scattering model (extinction and thermal diffuse scattering) tend to bias the atomic displacement parameters much more than the atomic positions. For these reasons, ADPs have to be – and have been – judged with some suspicion. However, it is evident that analysis of ADPs contains important information if these systematic errors are taken care of (Dunitz *et al.*, 1988; Dunitz & White, 1973; Bürgi & Capelli, 2000; Aree & Bürgi, 2006) and if the results can be confirmed by other techniques.

Unfortunately, complementary information about the thermal motion in crystals is seldom available from other experimental techniques. The dominating contribution to the ADPs comes from the low-frequency vibrations which are difficult to assess using Raman and IR spectroscopy. Inelastic neutron scattering is in principle able to derive the full phonon dispersion curves; however, this technique is neither easy to access, nor easy to apply for molecular crystals.

In the few cases where indisputably well measured ADPs have been compared with other experimental results, there has been a very good agreement. Our favourite examples are the comparison of the displacement parameters obtained from diffraction studies with results based on lattice-dynamical Born–von Karman models fitted to Raman and inelastic neutron scattering measurements. The results for urotropine (Willis & Howard, 1975) and silicon (Flensburg & Stewart, 1999) show a very good agreement between the diffraction experiments and the lattice-dynamical results. It is reasonable to assume that in many cases ADPs do really correspond to the mean-square displacements of the atoms in the crystal and are only slightly biased by other effects.

In the late 1970s and 1980s Gramaccioli and co-workers made important progress in the evaluation of temperature factors based on Born–von Karman lattice-dynamical force-field calculations (see *e.g.* Gramaccioli *et al.*, 1982). These studies showed a reasonable agreement with experimental temperature factors from neutron diffraction studies. In recent years, it has become feasible to derive the force constants for lattice-dynamical calculations of vibrational modes and ther-

modynamic properties from periodic DFT (density functional theory) calculations, and these types of calculations have been used intensively to investigate the vibrational and thermodynamic properties of mostly metals and inorganic materials (Baroni *et al.*, 2001).

There are well established methods for calculating mean-square displacements (MSDs) based on force-field calculations. There is a large amount of experimental material: the Cambridge Structural Database contains more than 500 000 structures of molecular crystals and a very large fraction of these have well determined ADPs. But very little work has been done to test the viability of *ab initio* methods to calculate the ADPs of molecular crystals. Morrison and co-workers (Reilly, Morrison & Rankin, 2011; Reilly, Morrison, Rankin & McLean, 2011) have used Car–Parrinello molecular dynamic (MD) simulations to investigate the anharmonic atomic motion in crystals. Based on their calculations, they suggest new models of anharmonic motion that will reduce the number of parameters typically used for these models (the Gram–Charlier). Nemkevich *et al.* (2010) used traditional force-field-based MD simulations to obtain isotropic harmonic motion. Comparing their results with experimental results, they generally observe that the computed MSDs are much smaller than the experimentally observed ones. Most recently, Dittrich *et al.* (2012) have used ONIOM (quantum mechanical/molecular mechanics hybrid) calculations to obtain ADPs for a number of molecular crystals. Their results compare well with experiments at ultra-low temperatures (10–20 K) when the computed ADPs are scaled against the observed ADPs. This is the study that is closest to the efforts described in the present paper and we devote some time to discussing the drawbacks and virtues of the two approaches (see below).

The calculation of ADPs for *molecular* crystals has additional challenges that are not found for extended solids. Whereas the dominant forces between the atoms in extended solids are strong and of covalent or ionic character, molecular crystals are held together by much weaker forces. In fact, dispersion forces may be dominant in systems without hydrogen-bonding capabilities. In these situations, current *ab initio* methods for solids, in particular the widely used DFT methods, may prove to be unable to quantitatively describe the dynamics of the system. In the present work, we test the use of an empirical dispersion term, proposed by Grimme (2006) and tested for crystalline systems (Civalleri *et al.*, 2008).

Even in the case where we trust the experimental ADPs as reflecting the MSDs of the atoms in the crystal, there are good reasons for striving to obtain a theoretical estimate of the MSDs. Three examples are discussed in the following.

1.1. Charge-density studies: hydrogen ADPs

It has long been recognized that the standard model in X-ray crystallography, the independent atom model, suffers from *asphericity shifts, i.e.* small errors in the atomic positions, as a consequence of inadequate modelling of the bonding density. The accuracy of the model of the atomic motion suffers from the same effect. These shortcomings can be circumvented by introducing the multipole formalism in order to describe the bonding density (Gatti & Macchi, 2012). Likewise, an inadequate description of the atomic motion will cause errors in the model of the static charge density. It is therefore important to have accurate displacement parameters for all atoms in the structure. Unfortunately this is not trivial for hydrogen atoms in X-ray-only charge-density studies, although in many cases hydrogen atoms play a key role in the system studied (Madsen, 2012), and previously a number of approaches have been investigated (Roversi & Destro, 2004; Madsen *et al.*, 2004; Madsen, 2006; Whitten & Spackman, 2006). A comparison of these different approaches with information from neutron diffraction experiments has been published (Munshi *et al.*, 2008). However, these approaches still require the use of the experimental ADPs for the non-hydrogen atoms in order to estimate the rigid-body vibrations of the molecule.

The fully periodic *ab initio* approach employed in the present study (Erba *et al.*, 2013) can be used to estimate the ADPs for hydrogen atoms, in a similar fashion as the TLS + ONIOM method (Whitten & Spackman, 2006), namely to use the *ab initio* calculations to estimate the internal vibrations and derive the external contribution from a TLS refinement. The internal contributions can also be obtained by computations on an isolated molecule; however, the lack of a crystalline environment is too severe an approximation, leading to much larger displacements than what is observed experimentally (Madsen *et al.*, 2003). However, a fully periodic approach can be used for much more than estimating internal vibrations, namely to include consistently long-range contributions and obtain the *total* MSDs for all atoms in the unit cell from the *ab initio* calculations. In contrast to the ONIOM approach (Whitten & Spackman, 2006), we can assess the dispersion of the low-frequency acoustic modes by using a supercell approach, which is crucial because the MSDs correspond to average displacements of all vibrational modes over the whole Brillouin zone (see §2.5).

Very recently, Dittrich *et al.* (2012) have used the ONIOM approach introduced by Whitten & Spackman to calculate not only the internal contribution to the ADPs, but also the low-frequency modes, to obtain total ADPs. Their approach is essentially an Einstein approximation, where a single molecule is allowed to move in the field of a static crystal lattice. They obtain good results, as judged from using the computed ADPs as fixed parameters in refinements against X-ray data, if the computed ADPs are scaled against the experimental results. Their approach was successful for the estimation of ADPs at very low temperatures (10–20 K). In the present study we go a step further to investigate the possibility of estimating ADPs at temperatures more commonly used in X-ray crystallography (100–123 K). The method employed in this study should be better at estimating the MSD at elevated temperatures, owing to the more elaborate description of the lattice vibrations – phonons – in the crystal.

1.2. Phonons

The ADPs provide three-dimensional information about the MSDs of atoms in crystals. However, they contain no information about the correlation of displacements of the individual atoms. Nevertheless, it is well known that atoms and molecules are moving in collective modes that extend throughout the crystal (phonons) and that there are also intramolecular correlated modes. Following the pioneering work of Cruickshank (1956*a*,*b*), researchers have analysed the ADPs as if they originated from collective motion with a considerable amount of success (see, *e.g.*, Schomaker & Trueblood, 1998; Dunitz *et al.*, 1988; Trueblood & Dunitz, 1983; Dunitz & White, 1973; He & Craven, 1985, 1993). The most well known model is the TLS model (Schomaker & Trueblood, 1968). More recently, Bürgi and co-workers have developed a multi-temperature approach that partly recovers the missing information about the correlated motion (Bürgi & Capelli, 2000; Capelli *et al.*, 2000; Bürgi *et al.*, 2002). However, in all these cases *a priori* knowledge or chemical intuition is crucial to proposing reasonable models of motion that can then be refined against the experimentally determined ADPs. In contrast, *ab initio* calculations require no other knowledge than the coordinates of the atoms in the structure, and may therefore provide fruitful information about the most important modes of correlated motion in a given system. Moreover, if the experimental and *ab initio* calculated ADPs are sufficiently close, we may argue that the dynamics derived from the calculations quantitatively reflect the dynamics in the real crystal.

1.3. Validation of *ab initio* approaches

Because of the inverse relationship between the frequency of normal modes and their contributions to the atomic MSD [equations (2) and (3), Fig. 1], the low-frequency phonons, corresponding to intermolecular motion, dominate the ADPs at ambient temperatures. The intermolecular forces are difficult to calculate using DFT methods, dominated as they are by weaker forces, as compared to the intramolecular covalent bonds.

A necessary condition for the calculated frequencies to be correct is a fair reproduction of the experimental results. The standard uncertainties of ADPs derived from standard X-ray diffraction work is less than 10^{-4} Å^2. Such a standard uncertainty should be taken with a pinch of salt; however, even if we consider the uncertainties to be several times higher, this is still a challenge for present-day *ab initio* methods, especially at ambient temperatures, as will be obvious from the results presented below.

Inelastic neutron scattering (INS) experiments can also be used to validate the *ab initio* calculations in a similar fashion as the comparison with ADPs derived from single-crystal diffraction techniques. Johnson *et al.* (2003) measured the INS spectrum from a polycrystalline sample of urea and compared it with the result of periodic DFT calculations. The comparison indicated that it was possible to assign the internal-mode spectrum, whereas there were large deviations for the external-mode spectrum, and it was only possible to obtain a reasonable agreement by fitting the acoustic modes to the experimental points measured by coherent INS on a single crystal of urea (Lefebfre *et al.*, 1975). The authors assign the lack of agreement between *ab initio* calculations and the INS spectrum to numerical errors in the calculations.

1.4. Outline of the paper

In the present paper we present results based on periodic HF (Hartree–Fock) and DFT calculations using the *CRYSTAL09* code (Dovesi *et al.*, 2005) to estimate both intramolecular *and* intermolecular vibrational contributions to the ADPs as applied to molecular crystals. Crystalline urea has been used as a case system. Based on the results for urea, the method has been further investigated with calculations on crystalline benzene, urotropine and L-alanine. As mentioned previously, it is interesting to compare both intra- and intermolecular vibrations to other methods. The four systems studied here have all been studied extensively using highly accurate X-ray and neutron diffraction experiments, as well as with spectroscopic techniques. In all cases, the ADPs from multi-temperature diffraction experiments have been analysed using normal-mode coordinate analysis by Bürgi and co-workers (Bürgi & Capelli, 2000; Capelli *et al.*, 2000; Bürgi *et al.*, 2002). For urea, benzene and urotropine we compare our *ab initio* results with the total ADPs as well as with the estimates of internal and external vibrations derived from the analysis of Bürgi and co-workers, and the spectroscopic results mentioned in their work. Finally, ADPs of L-alanine are reported as calculated at the B3LYP/6-31G(d,p) level of theory and compared with the available experimental data and computed results from Dittrich *et al.* (2012).

2. Methods

Calculations were carried out with the periodic *ab initio* *CRYSTAL09* program (Dovesi *et al.*, 2005, 2009).

2.1. Hamiltonians and basis sets

For urea, along with the HF method, five different DFT methods were adopted [the theoretical methods and basis sets are the same as previously adopted by one of us (Civalleri *et al.*, 2007)]: SVWN (Dirac, 1930; Vosko *et al.*, 1980), PW91 (Perdew, 1991) and the more recent GGA (generalized gradient approximation) functional PBE5, B3LYP (Becke, 1993; Lee *et al.*, 1988; Miehlich *et al.*, 1989) and PBE0 (Adamo & Barone, 1998) (also known as PBE1PBE). Four molecular all-electron basis sets were adopted: two from the Pople's family of basis set (Hehre *et al.*, 1986), namely, 6-31G(d,p) and 6-311G(d,p); a DZP basis set as proposed by Thakkar *et al.* (1993); and a TZP basis set devised by Ahlrichs and co-workers (Schäfer *et al.*, 1992). In the present work, comparison among HF and DFT methods was carried out by adopting the 6-31G(d,p) basis set, whereas the basis-set dependence of the results was investigated at the B3LYP level. The B3LYP method has also been augmented with an empirical dispersion

term as proposed by Grimme (2006) and modified for molecular crystals by Civalleri *et al.* (2008) (hereafter denoted as B3LYP-D*).

These comparisons were carried out using the urea molecular crystal as a test case. Based on a comparison of these results with experimental evidence, we adopted an approach based on both B3LYP/6-31G(d,p) at fixed lattice constants and B3LYP-D*/6-31G(d,p) for calculations on urotropine and benzene, as a compromise of accuracy and computational cost.

2.2. Computational parameters

The level of accuracy in evaluating the Coulomb and exchange series is controlled by five thresholds, for which values of 10^{-7}, 10^{-7}, 10^{-7}, 10^{-7}, 10^{-16} were used. The DFT exchange-correlation contribution is evaluated by numerical integration over the cell volume (Pascale *et al.*, 2004). Radial and angular points of the atomic grid are generated through Gauss–Legendre and Lebedev quadrature schemes. A grid pruning was adopted, as discussed in Pascale *et al.* (2004). In the present study a (75,974)p grid has been used that contains 75 radial points and a variable number of angular points, with a maximum of 974 on the Lebedev surface in the most accurate integration region. The condition for the SCF (self-consistent field) convergence was set to 10^{-8} on the total energy difference between two subsequent cycles. The shrinking factor of the reciprocal-space net was set to 4, corresponding to 18, 36, 16 and 36 reciprocal-space points of the irreducible Brillouin zone at which the Hamiltonian matrix was diagonalized, for urea, benzene, urotropine and L-alanine, respectively. The total energies obtained with this mesh are fully converged.

2.3. Geometry optimization

Starting from the experimental crystal structures (Swaminathan *et al.*, 1984; Jeffrey *et al.*, 1987; Kampermann *et al.*, 1995; Destro *et al.*, 1988), a full relaxation of both lattice parameters and atomic coordinates by means of analytical energy gradients was applied. Optimization of atomic coordinates while keeping the experimental lattice parameters was also tested (see below). Convergence is tested on the root mean square (RMS) and the absolute value of the largest component of the gradients and the estimated displacements. The threshold for the maximum force, the RMS force, the maximum atomic displacement and the RMS atomic displacement on all atoms have been set to 0.00045, 0.00030, 0.00180 and 0.00120 a.u., respectively. The optimization is considered complete when the four conditions are simultaneously satisfied. The crystal symmetry was maintained during the whole optimization process. Owing to significant expansion of the lattice parameters when the basis set is enlarged, we also computed ADPs by fixing the lattice parameters to the experimental values.

2.4. Vibrational frequencies and related properties

Harmonic vibrational frequencies were computed by diagonalizing the mass-weighted Hessian matrix (Pascale *et al.*, 2004). First derivatives with respect to nuclear coordinates are calculated analytically, whereas second derivatives are calculated numerically by finite displacements of the atomic positions. Since the energy variations for the displacements considered here can be as small as $10^{-6}/10^{-8}$ a.u., the tolerance on the energy convergence of the SCF cycles was set to 10^{-10} a.u. Calculations were carried out both at the Γ point and on a mesh of $\mathbf{q}$ points to properly sample the first Brillouin zone by means of a direct supercell approach. For the latter, a $2 \times 2 \times 2$ supercell was adopted which allows one to include 8 $\mathbf{q}$ points. This choice is a good compromise in the trade-off between cost and accuracy and provides good results.

As urea possesses a large dipole moment and is easily polarizable, longitudinal optical/transverse optical (LO–TO) splitting can occur. However, it has a small effect on the vibrational frequencies (Durman *et al.*, 1988) and will be neglected. Inclusion of the anharmonic correction (Ugliengo *et al.*, 2004) to high-frequency $-NH_2$ vibrational modes was tested, but hardly affects the ADPs, and was neglected.

Frequency shifts due to isotopic substitutions can readily be calculated, at no cost, by changing the masses in the mass-weighted Hessian matrix. This was done for benzene in order to compare with the experimental results, based on a deuterated system.

2.5. MSDs and ADPs

Once a stationary point on the potential energy surface has been found, the interatomic force-constant matrix can be obtained from the second partial derivatives of the potential energy. The forces can be used to form the dynamical matrix $D_{\alpha\alpha'}(kk'|\mathbf{q})$. An element of $\mathbf{D}$ is

$$D_{\alpha\alpha'}(kk'|\mathbf{q}) = [m(k)m(k')]^{-1/2} \sum_{l'} \Phi_{\alpha\alpha'} \begin{pmatrix} k & k' \\ 0 & l' \end{pmatrix} \times \exp[i\mathbf{q} \cdot \Delta\mathbf{r}(kk'l')], \quad (1)$$

where the $\Phi_{\alpha\alpha'}$'s are the corresponding components of force constants relative to the coordinates α and α', and $\Delta\mathbf{r}(kk'l')$ is the distance between the origins of asymmetric units.

The dynamical matrix can be diagonalized and the resulting eigenvectors $\mathbf{e}(j\mathbf{q})$ describe the atomic displacements of the mode $(j\mathbf{q})$. The eigenvalue corresponding to mode $(j\mathbf{q})$ is the (squared) normal-mode frequency $\omega_j(\mathbf{q})^2$.

The lowest frequencies normally correspond to the collective long-range translational and librational motion of the molecules in the crystal. Care must be taken to ensure that all frequencies are real and hence that the stationary point on the potential energy surface is a local minimum. A unit cell with N atoms has $3N$ degrees of freedom. With Z symmetry-related molecules in the unit cell, the $6Z$ lowest frequencies normally correspond to the translational and librational modes of the molecule. The remaining $3N - 6Z$ frequencies are then used to obtain the internal atomic MSDs, *assuming* that the overall molecular vibrations are uncoupled from the internal vibrations.

Once the normal modes and frequencies have been obtained, they can be used to calculate the vibrational

contributions to the thermodynamics of the crystal, *i.e.* the entropy and heat capacity. They can also be used to calculate the atomic MSD matrices and thereby the ADPs.

The atomic MSD matrix $\mathbf{B}_{\rm atom}(k)$ of a vibrating atom k may be written in terms of a summation of contributions from all the $3nN$ normal modes of vibration, where n is the number of atoms in the unit cell and N is the number of cells in the crystal:

$$\mathbf{B}_{\rm atom}(k) = \frac{1}{Nm_k}\sum_{j\mathbf{q}}\frac{E_j(\mathbf{q})}{\omega_j^2(\mathbf{q})}\mathbf{e}(k|\,j\mathbf{q})\mathbf{e}^*((k|\,j\mathbf{q}))^T, \qquad (2)$$

where $\mathbf{e}(k|\,j\mathbf{q})$ represents the kth component of a normalized complex eigenvector $\mathbf{e}(j\mathbf{q})$ and corresponds to atom k in normal mode j along the wavevector $\mathbf{q}$. ω_j is the frequency of mode j, m_k is the mass of atom k and $E_j(\mathbf{q})$ is the energy of the mode, given by

$$E_j(\mathbf{q}) = \hbar\omega_j(\mathbf{q})\left\{\frac{1}{2} + \frac{1}{\exp[\hbar\omega_j(\mathbf{q})/k_{\rm B}T] - 1}\right\}, \qquad (3)$$

where $k_{\rm B}$ is Boltzmann's constant. Once transformed to the possibly oblique coordinate system of the crystallographic unit cell, $\mathbf{B}_{\rm atom}(k)$ corresponds to the matrix of ADPs derived from structural refinement against crystallographic data.

2.5.1. Similarity index. We introduce a similarity index, as proposed by Whitten & Spackman (2006) in order to compare the total ADPs to the results obtained from neutron diffraction measurements. The index used by Whitten & Spackman is $S_{12} = 100(1 - R_{12})$ where

$$R_{12} = \int [p_1(\mathbf{v})p_2(\mathbf{v})]^{1/2}\,{\rm d}^3\mathbf{v} = \frac{2^{3/2}(\det \mathbf{U}_1^{-1}\mathbf{U}_2^{-1})^{1/4}}{[\det(\mathbf{U}_1^{-1} + \mathbf{U}_1^{-1})^{1/2}]}, \qquad (4)$$

p_1, p_2 are the probability density functions of the two atoms that are compared, and $\mathbf{U}_1, \mathbf{U}_2$ are the corresponding atomic MSD matrices. Because the probability density functions (p.d.f.'s) are normalized, $R_{12} = 1.0$ if $\mathbf{U}_1$ and $\mathbf{U}_2$ are identical, and therefore S_{12} is a measure of the percentage difference between the two p.d.f.'s – the smaller the value of S_{12}, the more similar the two p.d.f.'s are, and the closer the agreement between the ADPs $\mathbf{U}_1$ and $\mathbf{U}_2$. The similarity indices, based on the comparison between the neutron diffraction data and our estimates of the total ADPs, are given in the rightmost column of Tables 4, 8 and 9.

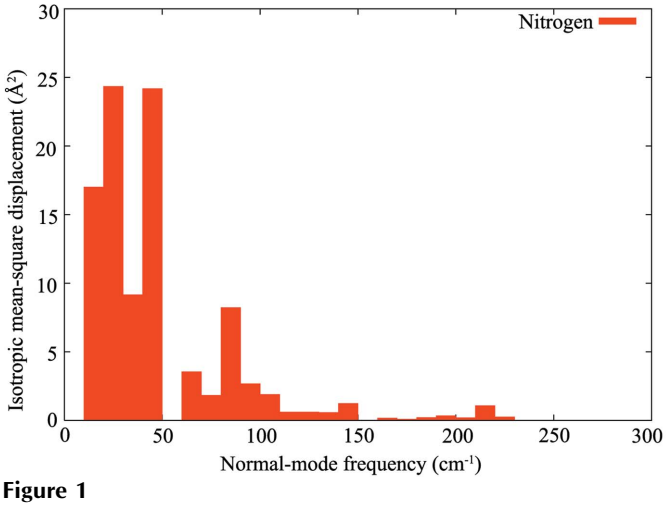

Figure 1
Contribution to the (isotropic) MSDs in crystalline urea (123 K) from the different normal modes, as a function of their frequency. The vibrational modes have been binned. Calculations were carried out at the B3LYP/6-31G(d,p) level.

Table 1
Urea: MSDs (10^{-4} Å^2) of internal modes of the C, N and O atoms as a function of the Hamiltonian.

The basis set is 6-31G(d,p) and the lattice parameters were fixed at the experimental values (Swaminathan *et al.*, 1984) at 15 K.

		MSD eigenvalues								
	Cell	C			N			O		
HF	exp	13	8	8	3	8	6	7	1	7
SVWN	exp	15	9	8	2	9	7	8	2	8
PW91	exp	15	9	8	2	9	7	8	2	8
PBE	exp	15	9	8	2	9	7	8	2	8
PBE0	exp	14	8	8	2	9	7	8	2	8
B3LYP	exp	15	9	8	2	9	7	8	2	8

3. Results and discussion

As described in §2.5, it is often sensible to divide the vibrational modes into internal and external modes. The external modes correspond to the overall motion of the molecules in the crystal and these modes are long-range vibrations with wavelengths extending through several unit cells. The frequencies of these modes vary with the wavelength; generally their frequencies are much smaller than the internal modes and thus increase with temperature. From 100 K upwards, the atomic MSDs of the non-hydrogen atoms mostly come from these external modes. An example for nitrogen in urea (123 K) is given in Fig. 1, where the internal modes play a somewhat larger role. Hydrogen atoms represent a special case because of their small mass and their MSDs have a large contribution from the internal modes even at room temperature. In the following, we divide the analysis into these two domains: the internal modes/low-temperature situation and the external modes/high-temperature scenario.

3.1. Urea

First we report and discuss results for crystalline urea, which is considered in the present work as a case study to assess theoretical methods and investigate the basis-set choice, as well as other computational parameters.

3.1.1. Internal modes. As shown in Table 1, the internal MSDs of the C, N and O atoms depend very little on the method and basis set adopted for the calculations. All the results are identical within 10^{-4} Å^2, which is well below the experimental uncertainty. Furthermore, they are in excellent agreement with spectroscopic data and previous calculations (Ishii & Scheringer, 1979; Rousseau *et al.*, 1998; Capelli *et al.*, 2000).

Because of their light mass, the H-atom internal displacements show larger deviations. In Table 2 we show the

Table 2
Urea: comparison of eigenvalues of the internal MSD matrix (10^{-4} Å^2) for H atoms computed with different theoretical methods, basis sets and supercell shape and size.

The frequencies were unscaled in the computation of MSDs. References: (1) Spectroscopic normal-mode analysis (Ishii & Scheringer, 1979). (2) *Ab initio* calculations (Rousseau *et al.*, 1998), obtained at the HF/6-31++G(d,p) level of theory with a scaling factor of 0.8. (3) Multi-temperature analysis of neutron data (Capelli *et al.*, 2000).

		MSD eigenvalues					
	Cell	H1			H2		
Hamiltonian [6-31G(d,p) basis]							
HF	exp	261	50	128	268	126	49
SVWN	exp	261	58	144	247	141	57
PW91	exp	288	56	142	276	140	55
PBE	exp	292	56	142	280	140	55
PBE0	exp	272	54	138	263	136	53
B3LYP	exp	280	54	138	269	136	53
Basis set (B3LYP functional)							
6-31G(d,p)	opt	287	54	140	266	136	54
6-311G(d,p)	opt	318	54	140	295	137	54
DZP	opt	292	55	143	275	140	54
TZP	opt	297	54	141	274	136	54
TZP	exp	273	54	137	269	136	54
Supercell approach [B3LYP/6-31g(d,p) method]							
111	opt	280	54	138	269	136	53
112	opt	286	53	140	269	136	52
221	opt	276	52	139	260	136	52
222	opt	274	52	139	260	135	52
222	exp	268	52	137	261	135	51
Spectroscopic (1)		245	54	134	240	134	54
Crystal field (2)		265	54	142	260	142	54
Neutron data (3)		263	66	120	263	120	66

dependence of the internal displacements on the DFT functional, basis set and the size of the supercell employed for the vibrational frequency calculations, and compare the results with previous investigations. The results are in good agreement with previous studies. A close inspection of the values reveals some trends. There is a decrease in the MSDs when going from the local density approximation (LDA) functionals to the GGA functionals. Likewise, there is a decrease in MSDs with increasing basis set, even though the optimized unit-cell size increases (see Table 3) with the basis set and thus partly compensates for this trend. Furthermore, when the supercell is enlarged, there is a noticeable decrease in the MSDs towards the spectroscopic results.

3.1.2. External modes and total ADPs. Because of the inverse relationship between the mode frequencies and the MSDs it is important to obtain a good estimate of the low-frequency translational and librational modes. This was pursued by applying a supercell approach. The atomic total MSDs were obtained by summing the MSDs corresponding to the different **q** vectors compatible with the supercell [equation (2)]. The results for urea using supercells with different size and shape are visualized by means of equal-probability ellipsoids in Fig. 2.

It is obvious from Fig. 2 that it is necessary to double all the lattice parameters in order to obtain results in reasonable agreement with experiment. A B3LYP/6-31G(d,p) calculation

Table 3
Urea: lattice parameters (in Å) and harmonic frequencies (in cm^{-1}) of the libration mode about the C—O bond.

Values are compared with results from: (1) Raman and INS (Lefebfre *et al.*, 1975), (2) force-field calculations (Parlinski & Chapuis, 1999) and (3) analysis of multi-temperature neutron diffraction data (Capelli *et al.*, 2000).

		Lattice parameters		Frequencies	
Method	Basis set	a	c	B_1	A_2
HF	6-31G(d,p)	5.94	4.75	41	48
PBE0	6-31G(d,p)	5.59	4.65	49	62
PBE	6-31G(d,p)	5.60	4.67	−9	50
PW91	6-31G(d,p)	5.60	4.66	21	56
SVWN	6-31G(d,p)	5.26	4.52	11	83
B3LYP	6-31G(d,p)	5.67	4.68	39	46
B3LYP	6-31G(d,p)	exp	exp	34	59
B3LYP	TZP	5.84	4.71	61	50
B3LYP	TZP	exp	exp	63	79
B3LYP-D*	TZP	5.54	4.67	73	95
Raman (100 K) (1)				61	
INS (1)				51	88
Force field (2)				20	105
Neutron diffraction (3)		5.57	4.68	64	

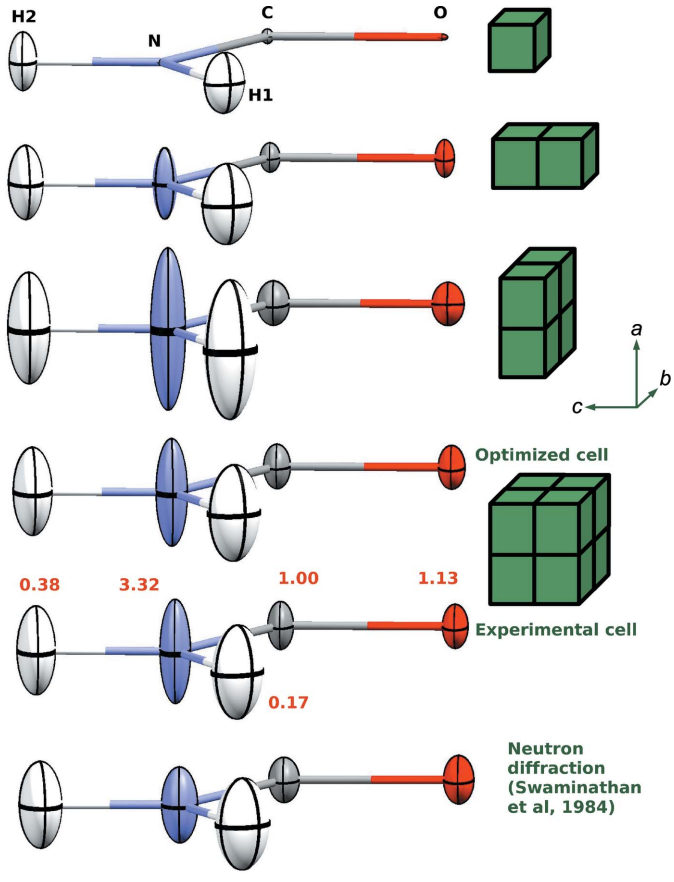

Figure 2
Urea: equal-probability ellipsoids (50%) of the symmetry-independent atoms as a function of supercell size (green boxes), compared with neutron diffraction data (Swaminathan *et al.*, 1984). Calculations using the B3LYP/6-31G(d,p) method. The red numbers indicate the similarity index between the calculations and the neutron diffraction result.

using a 2 × 2 × 2 supercell with experimental cell size is in qualitative agreement with the neutron diffraction model, apart from the nitrogen atom, which has displacements that are too large in the out-of-plane direction.

The supercell approach additionally allows the calculation of phonon dispersion curves. Fig. 3 shows the dispersion of urea along some of the principal directions in the first Brillouin zone. The results resemble previous curves based on fitting against INS measurements (Lefebfre *et al.*, 1975). There is a considerable gap in the dispersion curve at about 200 cm^{-1}. Above 200 cm^{-1} the frequencies show only little dispersion, corresponding primarily to the internal degrees of freedom, whereas the low-frequency modes depend very much on the length and direction of the wavevector, corresponding to external lattice vibrations. However, visualization of the different modes of vibration demonstrates that even for the lowest-frequency external modes there is some mixing with internal degrees of freedom; in particular, the motion of the hydrogen atoms is dampened by the intermolecular hydrogen bonding.

3.1.3. Out-of-plane displacement of nitrogen. The overestimation of the nitrogen displacements is related to librational modes about the axis coinciding with the C—O bond. These external librational modes are coupled with the internal pyramidalization of the NH_2 group, in agreement with the analysis of Capelli *et al.* (2000). The motion of the hydrogen atoms is thus dampened by the intermolecular interactions, but less so for the nitrogen atoms. The frequencies of these modes are very dependent on basis set, cell dimensions and functional, as evident from Table 3.

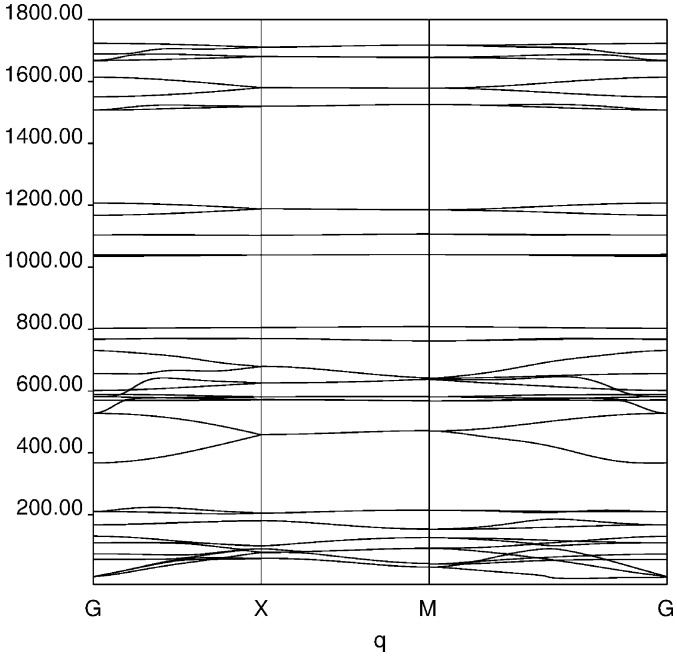

Figure 3
Phonon dispersion curves along principal directions of crystalline urea. The numbers on the ordinate are given in wavenumbers (cm^{-1}). Calculations were carried out at the B3LYP/TZP level. For clarity, N—H stretching phonon bands (around 3600 cm^{-1}) are not shown.

Table 4
Urea: ADPs (10^{-4} $Å^2$) from *ab initio* calculations as compared to the results of neutron diffraction experiments (fourth line) (Swaminathan *et al.*, 1984).

The calculations were B3LYP/6-31G(d,p) (first line) and B3LYP/TZP (second line) supercell (2 × 2 × 2) calculations fixing the cell to the 12 K experimental cell parameters, and the same calculation but with a Grüneisen parameter least-squares fitted to match the calculated ADPs with the observed ones. The scaling parameter was 0.81 at 12 K and 0.88 at 123 K.

	$U_{11} = U_{22}$	U_{33}	U_{12}	$U_{13} = U_{23}$	Similarity index
12 K					
C	48	29	−5	0	1.36
	44	30	−4	0	2.0
	55	37	−5	0	0.42
	63 (4)	35 (3)	2 (3)	0	
O	67	29	1	0	0.90
	65	30	−2	0	1.0
	81	37	−1	0	0.17
	87 (5)	32 (4)	2 (4)	0	
N	125	43	−81	3	1.7
	101	44	−60	4	1.6
	127	54	−75	4	0.51
	113 (3)	59 (2)	−52 (2)	4 (2)	
H1	237	167	−130	−24	0.50
	227	170	−122	−23	0.62
	281	210	−150	−28	0.12
	277 (9)	185 (7)	−143 (6)	−29 (8)	
H2	268	86	−83	12	0.65
	263	89	−80	13	0.57
	326	110	−99	16	0.17
	294 (8)	116 (6)	−94 (7)	15 (7)	
123 K					
C	156	46	−20	0	0.98
	115	49	−9	0	1.4
	145	60	−11	0	0.12
	147 (5)	65 (3)	1 (4)	0	
O	166	47	18	0	0.96
	139	49	12	0	1.9
	175	61	15	0	0.16
	197 (6)	63 (4)	17 (5)	0	
N	497	67	−366	1	3.63
	300	70	−200	2	1.4
	383	87	−257	2	1.1
	286 (4)	95 (2)	−147 (2)	2 (3)	
H1	446	200	−250	−30	0.13
	446	200	−250	−30	0.13
	351	205	−184	−27	0.42
	426	243	−223	−32	0.13
	440 (11)	216 (7)	−222 (8)	−31 (9)	
H2	441	110	−177	13	0.39
	379	115	−136	15	0.75
	456	138	−166	19	0.05
	430 (10)	140 (6)	−158 (8)	19 (8)	

Raman and INS measurements (Lefebfre *et al.*, 1975) indicate that the mode of symmetry B_1 has a frequency of approximately 56 cm^{-1} while the mode of symmetry A_2 has a frequency of approximately 88 cm^{-1}. The corresponding frequencies obtained using the 6-31G(d,p) basis set are generally lower than these values, no matter whether the optimized cell is larger or smaller than the experimental result.

When the cell is fixed at the experimental value, the B3LYP/6-31G(d,p) method still gives A_1 and B_1 frequencies smaller than the experimental values, and thus larger MSDs. In order to come close to experiment, we adopted a TZP basis set. Calculations were performed using the optimized cell as well

as the experimental cell. In both cases, we observed an enhancement of the frequencies towards the experimental results and the resulting MSD of the nitrogen atoms is in much better agreement with the results of the diffraction experiments: at 123 K (Table 4) the U_{11} parameter drops from 0.0497 to 0.0300 Å^2 on adoption of the TZP basis set and is now within four standard uncertainties of the neutron diffraction experiments.

In order to get an impression of the sensitivity of the calculated ADPs towards small changes in the frequencies of these modes, notice that a decrease of 5 wavenumbers for the mentioned out-of-plane librations about the C—O axis corresponds to an increase of 25% in the U_{11} parameter of nitrogen at 123 K, as illustrated in Fig. 4. This correspondence illustrates a general challenge in the calculation of the total ADPs, including the external lattice modes: it is the low-frequency modes that give the largest contribution to the MSDs [equations (2) and (3)], but these modes are largely determined by the weak, intermolecular forces, and are thus the most difficult to assess using *ab initio* approaches, as it requires a very precise estimate of the intermolecular potential energy surface. The expanding lattice is a consequence of the role of dispersive interactions in molecular crystals (see *e.g.* Civalleri *et al.*, 2007, 2008).

3.1.4. Empirical dispersion energy term. It is well known that there are problems with DFT methods in describing the dispersive interactions, and we investigated an approach to include an empirical dispersion term, based on the work by Grimme (2006) and described in a previous publication by one of us (Civalleri *et al.*, 2008). The urea structure was optimized at the B3LYP-D*/TZP level. The resulting lattice parameters were less than 0.5% from experiment; however, the frequencies of intermolecular modes become larger, as compared to a similar calculation without the empirical dispersion term. This results in atomic MSDs that are more than 20% lower than the experimental results. This result indicates that the adopted method gives a potential energy surface that is too steep, or that a harmonic potential is too crude an approximation of the true potential in the crystal.

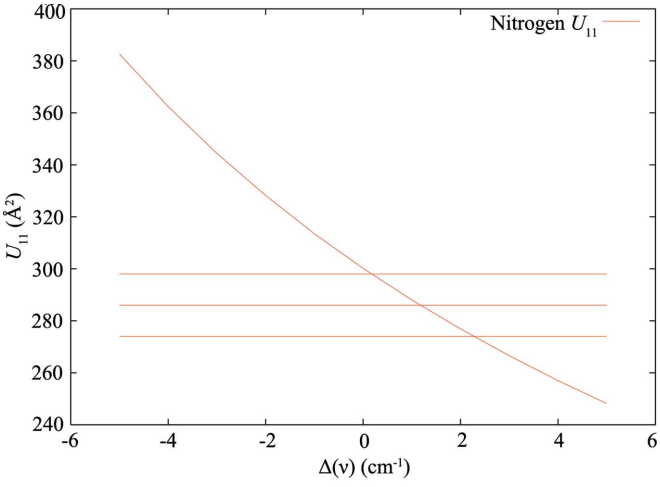

Figure 4
The variation of the U_{11} displacement parameter of the urea nitrogen atom as a function of the frequency of the mode describing the out-of-plane motion of the amino group. The horizontal lines correspond to the experimental result (middle line) and the experimental uncertainty (upper and lower lines deviate three standard uncertainties from the experimental value).

3.1.5. Summary for crystalline urea. In our experience, the methodology recommended to predict good-quality ADPs for crystalline urea – based on a comparison with the experimental data – is: (i) to adopt the B3LYP functional, (ii) to optimize the atomic positions while keeping fixed the experimental lattice parameters and (iii) to use a 2 × 2 × 2 supercell approach for vibrational frequencies calculations. Results for two different basis sets, namely, 6-31G(d,p) and TZP, are given in Table 4 at the temperatures 12 and 123 K. The experimental results based on neutron diffraction (Swaminathan *et al.*, 1984) are given for comparison. The third row for each atom in the tables represents scaled ADPs (see below).

Analysing these results in detail, we notice that at the lowest temperature (12 K) – where the internal modes play a significant role – the agreement is reasonably good for all atoms. As the temperature is increased (123 K), the external modes become important and the agreement is worse. The nitrogen atom, and the problems describing the libration about the C—O bond, represents a special case where the computed ADPs are higher than the experimental result. For the other atoms in urea, the trend is opposite: the computed ADPs are generally lower than the experimental ones.

As expected from the analysis of the librational modes, the TZP gives much better results for the nitrogen ADPs as compared to the 6-31G(d,p) basis. However, the dampening of the out-of-plane libration also affects the ADPs of the hydrogen atoms that are now in slightly worse agreement with experiment.

In most cases, off-diagonal elements of the ADPs are within a few standard uncertainties of the experimental results. The differences are mostly found in the overall size of the MSDs and there is a clear trend that the calculated MSDs are smaller than the ones derived from experiment.

In summary, from Tables 1, 2 and 4, we conclude that the contribution to the MSDs coming from the internal vibrational modes is more or less independent of the basis-set size and DFT functional, and the widely used B3LYP/6-31G(d,p) method can be adopted for obtaining these internal vibrations. For the best possible estimate, including also external modes, at least a 2 × 2 × 2 supercell has to be employed.

3.2. Benzene and urotropine

The computational strategy proposed above was then applied to solid benzene and urotropine. The two systems were selected because of the availability of accurate experimental data from multi-temperature analysis of neutron diffraction measurements.

3.2.1. Internal modes. As for urea, the MSDs corresponding to internal vibrations are in excellent agreement with previous calculations and experimental evidence (see Tables 5, 6 and 7).

Table 5
Benzene: *internal* MSDs (units 10^{-4} Å^2).

Computational level: 2 × 2 × 2 supercell, B3LYP/6-31G(d,p). Compared to a force-field derived from spectroscopic measurements and results derived from multi-temperature analysis (Capelli *et al.*, 2000) of neutron diffraction measurements (Jeffrey *et al.*, 1987).

	ε_{11}	ε_{22}	ε_{33}	ε_{12}	ε_{13}	ε_{23}
	C			H/D		
C_6H_6						
Periodic *ab initio* calculations	7	11	12	54	114	172
Spectroscopic force field	9	12	14	61	130	202
ADP analysis	14 (1)	11 (1)	11 (1)	68 (2)	124 (2)	171 (3)
C_6D_6						
Periodic *ab initio* calculations	14	7	11	39	78	115
Spectroscopic force field	13	8	16	44	89	133
ADP analysis	14 (1)	7 (1)	15 (1)	52 (2)	83 (2)	110 (3)

Table 6
Urotropine: calculated MSD amplitudes (units 10^{-4} Å^2) from *internal* high-frequency vibrations for nitrogen and carbon.

Computational level: 2 × 2 × 2 supercell, B3LYP/6-31G(d,p). Compared to vibrational analysis of IR and Raman spectroscopic data (Cyvin, 1972).

	T (K)	ε_{11}(N)	ε_{22}(N)	ε_{11}(C)	ε_{22}(C)	ε_{33}(C)
Vibrational analysis from IR and Raman	0	13	10	15	12	16
Periodic *ab initio* calculations	15	15	11	15	13	15
Vibrational analysis from IR and Raman	298	15	12	16	15	19
Periodic *ab initio* calculations	298	16	12	17	15	17

Table 7
Urotropine: calculated MSD amplitudes (units 10^{-4} Å^2) from *internal* high-frequency vibrations for hydrogen.

Computational level: 2 × 2 × 2 supercell, B3LYP/6-31G(d,p). Compared to multi-temperature normal-mode analysis (Capelli *et al.*, 2000), vibrational analysis of IR and Raman spectroscopic data (Cyvin, 1972) and INS measurements (Thomas & Ghosh, 2012).

	T (K)	ε_{11}	ε_{22}	ε_{33}	ε_{13}
ADP analysis	15–298	65 (1)	136 (1)	165 (1)	4 (1)
Vibrational analysis, IR and Raman	0	68	141	237	5
Periodic *ab initio* calculations	15	73	130	173	3
INS	100	68	129	204	5
Periodic *ab initio* calculations	100	73	130	173	3
Periodic *ab initio* calculations	298	67	151	187	12
Vibrational analysis, IR and Raman	298	72	146	275	12

Because these internal modes dominate at low temperature, there is also very nice correspondence with neutron diffraction experiments at the lowest temperatures, especially if we introduce a correction for anharmonicity (see below).

Table 8
Benzene, deuterated.

The first line in each group of four lines corresponds to computed ADPs based on B3LYP/6-31G(d,p) calculations with a 2 × 2 × 2 supercell; the second line corresponds to a 2 × 2 × 2 supercell B3LYP-D*/6-31G(d,p) calculation; the third line corresponds to the same calculations as the second line, but with an overall scaling of frequencies, corresponding to a least-squares minimization against the experimental ADPs. The scaling factor was 0.74 for the 15 K model and 0.76 for the 123 K model. The fourth line gives ADPs derived from neutron diffraction data (Jeffrey *et al.*, 1987).

	U_{11}	U_{22}	U_{33}	U_{12}	U_{13}	U_{23}	Similarity index
15 K							
C1	68	52	72	6	2	1	0.83
	60	49	64	6	2	1	1.54
	80	65	84	9	2	0	0.11
	79 (2)	67 (2)	88 (2)	6 (2)	7 (2)	4 (1)	
C2	64	71	63	6	14	−1	0.56
	58	64	60	6	14	−1	1.06
	76	86	78	9	18	−2	0.04
	74 (2)	81 (2)	79 (2)	9 (2)	17 (2)	0 (2)	
C3	68	63	69	−3	11	13	0.68
	61	58	59	−2	8	9	1.43
	80	77	78	−4	10	13	0.06
	81 (2)	75 (2)	82 (2)	−3 (2)	14 (2)	10 (1)	
D1	198	95	214	44	19	10	0.43
	182	91	194	42	16	9	0.61
	224	112	240	52	18	10	0.05
	224 (3)	114 (2)	239 (3)	46 (2)	25 (2)	12 (2)	
D2	162	192	171	39	81	−3	0.53
	153	176	165	35	80	−3	0.61
	189	219	204	44	99	−5	0.13
	183 (2)	204 (3)	208 (3)	35 (2)	88 (2)	−8 (2)	
D3	200	156	185	−11	62	72	0.52
	182	142	158	−15	49	58	0.63
	225	177	196	−19	60	72	0.14
	214 (3)	171 (2)	199 (3)	−18 (2)	61 (2)	58 (2)	
123 K							
C1	177	146	187	0	14	−6	1.88
	140	127	148	1	−13	−8	4.6
	228	208	242	17	−24	−14	0.09
	232 (3)	200 (3)	262 (3)	17 (3)	−13 (3)	−12 (3)	
C2	165	204	158	4	19	−10	1.93
	132	170	137	10	19	−10	4.4
	215	281	222	19	31	−19	0.11
	218 (3)	255 (3)	242 (3)	14 (3)	33 (3)	−16 (3)	
C3	177	183	182	24	14	36	1.62
	140	151	137	−13	5	18	4.3
	227	250	224	−25	6	30	0.08
	230 (3)	237 (3)	233 (3)	−22 (3)	17 (3)	19 (3)	
D1	378	199	419	63	−4	3	0.41
	312	176	336	66	−8	−1	2.3
	470	270	507	99	−25	−6	0.07
	472 (5)	262 (3)	519 (6)	83 (3)	2 (5)	−2 (4)	
D2	313	417	311	71	129	−13	0.68
	267	342	285	60	123	−15	2.9
	403	530	431	92	183	−26	0.18
	400 (5)	469 (5)	449 (5)	69 (4)	168 (5)	−32 (5)	
D3	379	344	387	−36	104	162	0.71
	312	278	280	−39	62	102	2.7
	469	430	424	−65	86	156	0.11
	450 (5)	400 (5)	428 (5)	−63 (4)	91 (5)	124 (4)	

3.2.2. External modes and total ADPs. We observe similar trends for benzene and urotropine as for urea. The best agreement is observed at the lowest temperatures. At elevated temperatures the agreement with experimental evidence is less good (see Tables 8 and 9). Plots of thermal ellipsoids showing the agreement with experimental results are given in

Table 9
Urotropine: ADPs at 15 and 200 K.

The first line in each group of four lines corresponds to computed ADPs based on B3LYP/6-31G(d,p) calculations with a 2 × 2 × 2 supercell. The second line corresponds to a 2 × 2 × 2 supercell B3LYP-D*/6-31G(d,p) calculation. The third line corresponds to the same calculations as the second line, but with an overall scaling of frequencies, corresponding to a least-squares minimization against the experimental ADPs. The scaling factor was 0.89 for the 15 K model and 0.59 for the 123 K model. The fourth line gives ADPs derived from neutron diffraction data (Kampermann *et al.*, 1995). Units are 10^4 Å^2.

	U_{11}	U_{22}	U_{33}	U_{12}	U_{23}	Similarity index
15 K						
C	31		53		−2	0.37
	29		48		−1	0.71
	33		53		−1	0.43
	27 (3)		60 (2)		2 (3)	
N	40			−5		1.38
	37			−4		1.63
	41			−4		1.52
	43 (2)			−11 (2)		
H	158	182		54	9	0.38
	153	172		49	12	0.60
	171	193		55	14	0.29
	151 (6)	214 (5)		57 (4)	20 (5)	
200 K						
C	84		167		−5	10.6
	71		133		1	16.0
	180		351		4	0.27
	155 (4)		388 (4)		2 (6)	
N	124			−20		6.4
	101			−16		16.0
	266			−43		0.42
	280 (3)			−67 (2)		
H	233	358		89	7	8.10
	208	299		71	18	10.9
	439	700		161	30	0.35
	353 (9)	731 (10)		143 (8)	39 (11)	

Figs. 5 and 6. In agreement with the results for urea, we find that the calculated ADPs are significantly lower than the experimental results, and that it is the diagonal elements of the ADP tensor that show the largest discrepancies. The discrepancies can be described as some sort of scaling problem.

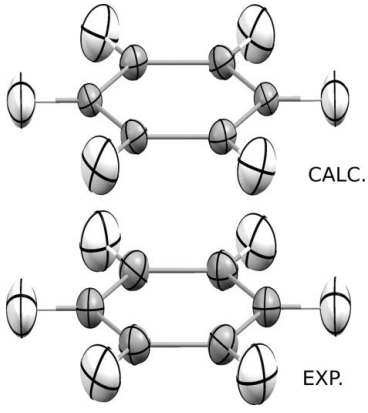

Figure 5
Benzene: equal-probability ellipsoids (50%) comparing the experimental and *ab initio* calculated ADPs at 123 K. Calculations were carried out at the B3LYP/6-31G(d,p) level by using a 2 × 2 × 2 supercell.

These deviations cannot be caused by a lack of correction for thermal diffuse scattering or extinction effects in the crystals, because this biases the experimental ADPs towards values that are too small (Blessing, 1995).

However, the use of lattice parameters derived from the low-temperature diffraction studies becomes an approximation at higher temperatures. The smaller cell volume leads to a steeper potential energy surface and thus to smaller displacements.

The differences could correspond to a potential energy surface that is too steep in the region around the minimum, or they might arise because the intermolecular potential is very far from harmonic, while a basic assumption in the calculations is a harmonic potential.

The differences can further come from the inability of the DFT calculations to describe the weak intermolecular forces in benzene and urotropine. As for urea, an empirical dispersion correction term was included, with very similar results. The differences between the observed and calculated ADPs become larger as the calculated ADPs become smaller. The dispersion term adds a positive contribution to the intermolecular forces and thereby increases the frequencies of the normal modes.

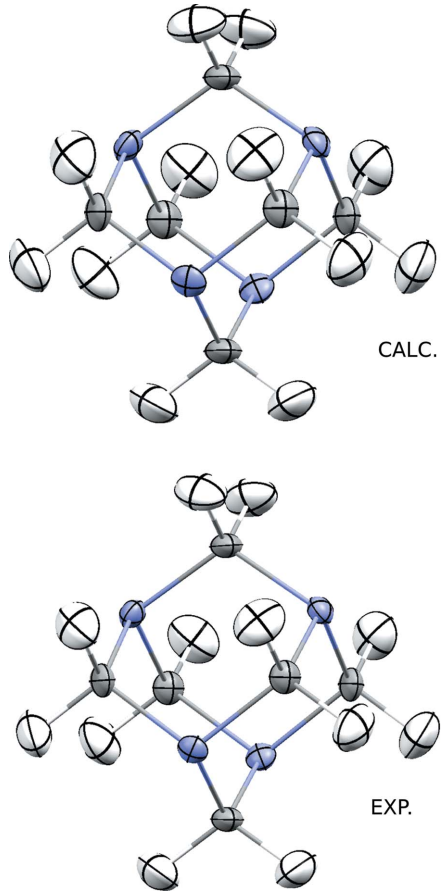

Figure 6
Urotropine: equal-probability ellipsoids (50%) comparing the experimental and *ab initio* calculated ADPs at 200 K. Calculations were carried out at the B3LYP/6-31G(d,p) level by using a 2 × 2 × 2 supercell.

3.3. Anharmonicity correction

The thermal expansion of the urea, benzene and urotropine crystal lattices indicates anharmonicity. Bürgi *et al.* (2000) have studied the anharmonicity of crystalline urotropine by the analysis of multiple-temperature neutron diffraction data. They refined a Grüneisen parameter γ_G defined as

$$\gamma_G = \left(1 - \frac{\omega_{eff}}{\omega_0}\right)\frac{V_{min}}{\Delta V}, \quad (5)$$

where ω_{eff} is the effective frequency, ω_0 is the original harmonic frequency, V_{min} is the volume at the lowest available temperature and ΔV is the volume difference between the lowest available temperature and the temperature of interest. Bürgi and co-workers found values for urotropine in the range γ_G = 2–5, depending on the model employed. Correcting our computed frequencies using a value of 5 for the Grüneisen parameter significantly improves the model as compared to the experimental data and this prompted us to investigate the possibility of anharmonic corrections further.

A least-squares fitting procedure was employed to find the best Grüneisen parameter that minimizes the mean S value between observed and calculated atomic MSDs for the highest measurement temperatures of the three systems. The Grüneisen parameters refine to values of 16.4 for urotropine (200 K), 9.9 for benzene (123 K) and 15.6 for urea (120 K), higher than what is observed experimentally. The resulting similarity indices become in all cases much lower than without the anharmonicity correction. (The resulting ADPs are given in Tables 4, 8 and 9.) Notice that the similarity indices for the hydrogen atoms are in all cases comparable to the results obtained using the approaches based on TLS analysis combined with internal motion (Munshi *et al.*, 2008).

Given the very large Grüneisen parameters needed to obtain a satisfactory agreement with experiment, we conclude that anharmonicity can explain some, but not all of the discrepancies between the computed and observed MSDs. The refined Grüneisen parameters correspond to scaling factors for the frequencies in the range 0.76–0.91. The scaling factors are lower than values found by comparing calculated frequencies for isolated molecules with fundamental frequencies found spectroscopically (Scott & Radom, 1996). It is, however, not straightforward to compare these values, because the present scale factors are dominated by the contributions from intermolecular low-frequency modes. These modes are only partly present in gas-phase studies, and furthermore are hard to obtain from Raman and below-red spectroscopies.

3.4. A test on L-alanine

We end the analysis by making a comparison to the related study by Dittrich *et al.* (2012). To do so, we chose the L-alanine crystal. As for the procedure set up above for other systems, calculations were performed at the B3LYP-D/6-31G(d,p) level using a 2 × 2 × 2 supercell and starting from the geometry found by Destro *et al.* (1988) at 23 K. The geometry of the molecules was then optimized, whereas the cell constants were fixed at the experimental values. The ADPs of the non-hydrogen atoms are given in Table 10. The hydrogen ADPs reported by Destro are estimated parameters based on a combination of rigid-body analysis and internal vibrations from spectroscopic studies (Roversi & Destro, 2004). A comparison of the thermal ellipsoids based on the work by Destro and the computed ADPs is given in Fig. 7.

Table 10
L-Alanine: ADPs (10^{-5} Å^2) from *ab initio* calculations as compared to the results of X-ray diffraction experiments (second line of each group) (Destro *et al.*, 1988).

The calculations were carried out at the B3LYP/6-31G(d,p) level by using a supercell approach (2 × 2 × 2) and fixing the cell to the 23 K experimental cell parameters. The second line of each group shows the calculated results using scaled frequencies. The scale factor was 0.94.

	U_{11}	U_{22}	U_{33}	U_{12}	U_{13}	U_{23}	Similarity index
C1	445	356	333	40	−21	−6	0.46
	481	382	358	42	−23	−6	0.34
	458 (9)	457 (8)	331 (10)	79 (8)	−12 (8)	−23 (8)	
C2	452	382	354	39	−24	−4	0.31
	488	409	381	42	−26	−5	0.14
	494 (9)	464 (9)	360 (11)	47 (8)	−35 (8)	8 (8)	
C3	556	726	601	−132	−54	−28	0.22
	600	777	646	−141	−58	−30	0.14
	569 (9)	866 (9)	604 (11)	−141 (8)	−70 (8)	−39 (8)	
N1	506	505	388	10	32	−8	0.24
	546	541	417	11	33	−9	0.11
	545 (8)	592 (7)	404 (9)	10 (6)	61 (7)	−19 (6)	
O1	615	638	566	255	−45	57	0.06
	664	685	609	273	−48	61	0.04
	647 (9)	662 (9)	588 (12)	260 (8)	−74 (9)	46 (9)	
O2	669	652	372	189	35	−50	0.17
	722	699	400	202	37	−54	0.07
	727 (10)	725 (9)	395 (11)	207 (9)	58 (9)	−74 (8)	

A multipole model was refined against the X-ray data using the program *VALRAY* (Stewart *et al.*, 1998). Scattering factors were constructed in the same way as in our recent charge-density study (Madsen *et al.*, 2011). The multipole expansion was truncated at the octupole level for the C, N and O atoms, and at the quadrupole level for the H atoms. H-atom nuclear parameters were fixed at the values used by Destro *et al.* No radial parameters were refined. The model was refined against F^2, and the final residuals were R = 2.2%, $wR(F^2)$ =

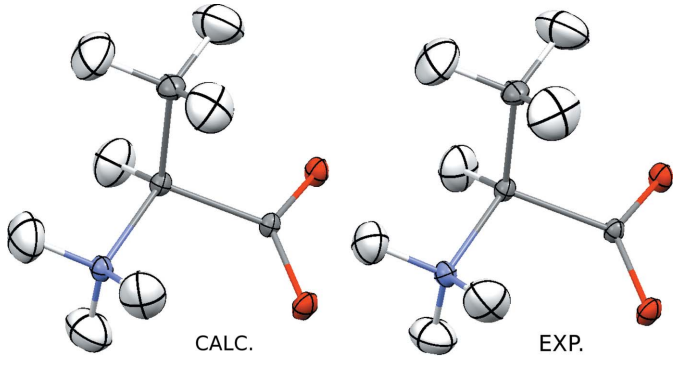

Figure 7
L-Alanine: equal-probability ellipsoids (75%) comparing the experimental and *ab initio* calculated ADPs at 200 K. Calculations were carried out at the B3LYP/6-31G(d,p) level by using a 2 × 2 × 2 supercell.

3.6% and goodness of fit GOF = 1.3. The $R(F)$ is slightly higher than that reported by Dittrich, reflecting the fact that the charge-density models are not entirely the same and the fact that we are refining against F^2 instead of F.

Incorporating the ADPs obtained from *ab initio* modelling as fixed parameters in the multipole model gives a fit with residuals R = 2.40%, $wR(F^2)$ = 3.97% and GOF = 1.42. A scaling of frequencies to optimize the agreement with the observed ADPs was tried. The frequency scaling factor becomes 0.93, but the changes in residuals were very modest [R = 2.35%, $wR(F^2)$ = 3.85%, GOF = 1.39]. These changes were accompanied by a significant drop in the mean similarity index, from 0.24 to 0.14.

We conclude that the computed ADPs can be used without any scaling in this case, probably as a consequence of the low temperature where the influence of thermal motion is much less important than at elevated temperatures.

4. Conclusion

We have demonstrated that the internal MSDs obtained from periodic HF and DFT calculations can be obtained in excellent agreement with experiments, making way for the use in *e.g.* experimental charge-density studies *via* a combined periodic *ab initio* calculations and TLS approach. A benchmark study of such an *ab initio* + TLS approach on a range of relevant compounds will be described in a forthcoming paper.

The successful calculation of internal modes also paves the way for accurately estimating the total ADPs at very low temperatures (10 K), because at this temperature the external modes give a less significant contribution. This was demonstrated by the successful use of computed total ADPs in a model refined against X-ray data for L-alanine at 23 K.

The calculation of total MSD matrices for molecular crystals through lattice dynamics can be demanding but computed results contain a lot of relevant additional information such as vibrational frequencies, zero-point energy and thermodynamic properties. The external-mode frequencies are very sensitive to changes in the DFT functional and basis set. We generally find that the calculated ADPs are smaller than the experimental results. An exception is the mode describing the libration about the C—O axis in urea, where a more elaborate basis set is needed to describe the potential energy surface and thereby reduce the size of the calculated out-of-plane displacement.

Most of the discrepancies can be removed by including a Grüneisen correction for anharmonicity; however, since this correction is larger than what would be expected based on other experimental evidence, it is likely that part of the discrepancy is due to other computational aspects than the harmonic approximation. The potential energy surface, as obtained from the periodic *ab initio* approach described here, appears to be too steep. Including an empirical dispersion energy correction in the calculations only enhances these discrepancies.

Instead of the Grüneisen approach, an anharmonicity correction to the ADPs due to the expanding lattice can also be obtained directly from the *ab initio* calculations by varying the cell volume in a quasi-harmonic approximation. This approach will be the subject of forthcoming work.

The scaled results for hydrogen atoms become comparable to – or even better than – the results obtained by the approaches where TLS analysis is combined with internal motion (Munshi *et al.*, 2008).

Our results indicate that the B3LYP method combined with a standard basis set [*i.e.* 6-31G(d,p)] provides good results when the lattice parameters are fixed at the experimental values. For internal motion, good-quality ADPs can be obtained by referring to the single unit cell while, in most cases, a 2 × 2 × 2 supercell is enough to obtain intermolecular force constants of a sufficient quality to give a good estimate of the total ADPs of all atoms. As the temperature increases, it becomes crucial to scale the normal-mode frequencies in order to take anharmonic effects into account.

The calculation of ADPs and their comparison with accurate experimental data may stimulate further development in the *ab initio* lattice dynamics of molecular crystals because they demonstrate a straightforward way to validate the theoretical methods. *Ab initio* calculations can also be the first step in an alternative approach to a lattice-dynamical model of the molecular motion in refinement against diffraction data.

We are grateful to Professor Sine Larsen for encouragement, comments and suggestions regarding this work, and to Professor Riccardo Destro for providing the structure-factor amplitudes from the L-alanine X-ray diffraction experiment. The Danish Council for Independent Research is acknowledged for financial support.

References

Adamo, C. & Barone, V. (1998). *Chem. Phys. Lett.* **298**, 113–119.
Aree, T. & Bürgi, H.-B. (2006). *J. Phys. Chem. B*, **110**, 26129–26134.
Baroni, S., de Gironcoli, S., Dal Corso, A. & Giannozzi, P. (2001). *Rev. Mod. Phys.* **73**, 515–562.
Becke, A. D. (1993). *J. Chem. Phys.* **98**, 5648–5652.
Blessing, R. H. (1995). *Acta Cryst.* B**51**, 816–823.
Bürgi, H. B. & Capelli, S. C. (2000). *Acta Cryst.* A**56**, 403–412.
Bürgi, H. B., Capelli, S. C. & Birkedal, H. (2000). *Acta Cryst.* A**56**, 425–435.
Bürgi, H.-B., Capelli, S. C., Goeta, A. E., Howard, J. A. K., Spackman, M. A. & Yufit, D. S. (2002). *Chem. Eur. J.* **8**, 3512–3521.
Capelli, S. C., Förtsch, M. & Bürgi, H. B. (2000). *Acta Cryst.* A**56**, 413–424.
Civalleri, B., Doll, K. & Zicovich-Wilson, C. (2007). *J. Phys. Chem. B*, **111**, 26–33.
Civalleri, B., Zicovich-Wilson, C. M., Valenzano, L. & Ugliengo, P. (2008). *CrystEngComm.* **10**, 405–410.
Cruickshank, D. W. J. (1956*a*). *Acta Cryst.* **9**, 754–756.
Cruickshank, D. W. J. (1956*b*). *Acta Cryst.* **9**, 1010–1011.
Cyvin, S. J. (1972). *Molecular Structures and Vibrations: Selected Contributions to Theoretical and Experimental Studies of Polyatomic Molecules by Spectroscopic Methods and Gas Electron Diffraction.* New York: Elsevier Publishing Co.
Destro, R., Marsh, R. & Bianchi, R. (1988). *J. Phys. Chem.* **92**, 966–973.
Dirac, P. A. M. (1930). *Proc. Cambridge Philos. Soc.* **26**, 376–385.

Dittrich, B., Pfitzenreuter, S. & Hübschle, C. B. (2012). *Acta Cryst.* A**68**, 110–116.
Dovesi, R., Orlando, R., Civalleri, B., Roetti, C., Saunders, V. R. & Zicovich-Wilson, C. M. (2005). *Z. Kristallogr.* **220**, 571–573.
Dovesi, R., Saunders, V. R., Roetti, C., Orlando, R., Zicovich-Wilson, C. M., Pascale, F., Civalleri, B., Doll, K., Harrison, N. M., Bush, I. J., D'Arco, P. & Llunell, M. (2009). *CRYSTAL09 User's Manual*, 1st ed. University of Torino, Italy.
Dunitz, J. D., Maverick, E. F. & Trueblood, K. N. (1988). *Angew. Chem. Int. Ed. Engl.* **27**, 880–895.
Dunitz, J. D. & White, D. N. J. (1973). *Acta Cryst.* A**29**, 93–94.
Durman, R., Jayasooriya, U. A. & Kettle, S. F. A. (1988). *J. Phys. Chem.* **92**, 620–622.
Erba, A., Ferrabone, M., Orlando, R. & Dovesi, R. (2013). *J. Comput. Chem.* **34**, 346–354.
Flensburg, C. & Stewart, R. F. (1999). *Phys. Rev. B*, **60**, 284–290.
Gatti, C. & Macchi, P. (2012). *Modern Charge-Density Analysis*, 1st ed. Heidelberg: Springer.
Gramaccioli, C. M., Filippini, G. & Simonetta, M. (1982). *Acta Cryst.* A**38**, 350–356.
Grimme, S. (2006). *J. Comput. Chem.* **27**, 1787–1799.
He, X. M. & Craven, B. M. (1985). *Acta Cryst.* A**41**, 244–251.
He, X.-M. & Craven, B. M. (1993). *Acta Cryst.* A**49**, 10–22.
Hehre, W. J., Radom, L., Schleyer, P. V. R. & Pople, J. A. (1986). *Ab Initio Molecular Orbital Theory.* New York: Wiley.
Ishii, M. & Scheringer, C. (1979). *Acta Cryst.* A**35**, 613–616.
Jeffrey, G. A., Ruble, J., McMullan, R. & Pople, J. A. (1987). *Proc. R. Soc. London Ser. A*, **414**, 47–57.
Johnson, M. R., Parlinski, K., Natkaniec, I. & Hudson, B. S. (2003). *Chem. Phys.* **291**, 53–60.
Kampermann, S. P., Sabine, T. M., Craven, B. M. & McMullan, R. K. (1995). *Acta Cryst.* A**51**, 489–497.
Lee, C., Yang, W. & Parr, R. G. (1988). *Phys. Rev. B*, **37**, 785–789.
Lefebfre, J., More, M., Fouret, R., Hennion, B. & Currat, R. (1975). *J. Phys. C*, **8**, 2011–2021.
Madsen, A. Ø. (2006). *J. Appl. Cryst.* **39**, 757–758.
Madsen, A. Ø. (2012). *Modeling and Analysis of Hydrogen Atoms*, Vol. 146 of *Structure and Bonding.* Berlin, Heidelberg: Springer.
Madsen, A. Ø., Mason, S. & Larsen, S. (2003). *Acta Cryst.* B**59**, 653–663.
Madsen, A. Ø., Mattson, R. & Larsen, S. (2011). *J. Phys. Chem. A*, **115**, 7794–7804.
Madsen, A. Ø., Sørensen, H. O., Flensburg, C., Stewart, R. F. & Larsen, S. (2004). *Acta Cryst.* A**60**, 550–561.
Miehlich, B., Savin, A., Stoll, H. & Preuss, H. (1989). *Chem. Phys. Lett.* **157**, 200–206.
Munshi, P., Madsen, A. Ø., Spackman, M. A., Larsen, S. & Destro, R. (2008). *Acta Cryst.* A**64**, 465–475.
Nemkevich, A., Bürgi, H.-B., Spackman, M. A. & Corry, B. (2010). *Phys. Chem. Chem. Phys.* **12**, 14916–14929.
Parlinski, K. & Chapuis, G. (1999). *J. Chem. Phys.* **110**, 6406–6411.
Pascale, F., Zicovich-Wilson, C. M., Lopez Gejo, F., Civalleri, B., Orlando, R. & Dovesi, R. (2004). *J. Comput. Chem.* **25**, 888–897.
Perdew, J. P. (1991). *Electronic Structure of Solids*, edited by P. Ziesche & H. Eschrig, pp. 11–20. Berlin: Akademie Verlag.
Reilly, A. M., Morrison, C. A. & Rankin, D. W. H. (2011). *Acta Cryst.* A**67**, 336–345.
Reilly, A. M., Morrison, C. A., Rankin, D. W. H. & McLean, K. R. (2011). *Acta Cryst.* A**67**, 346–356.
Rousseau, B., Van Alsenoy, C., Keuleers, R. & Desseyn, H. O. (1998). *J. Phys. Chem. A*, **102**, 6540–6548.
Roversi, P. & Destro, M. (2004). *Chem. Phys. Lett.* **386**, 472–478.
Schäfer, A., Horn, H. & Ahlrichs, R. (1992). *J. Chem. Phys.* **97**, 2571–2577.
Schomaker, V. & Trueblood, K. N. (1968). *Acta Cryst.* B**24**, 63–76.
Schomaker, V. & Trueblood, K. N. (1998). *Acta Cryst.* B**54**, 507–514.
Scott, A. P. & Radom, L. (1996). *J. Phys. Chem.* **100**, 16502–16513.
Stewart, R. F., Spackman, M. & Flensburg, C. (1998). *VALRAY98 Users' Manual.* Carnegie Mellon University, USA, and University of Copenhagen, Denmark.
Swaminathan, S., Craven, B. M. & McMullan, R. K. (1984). *Acta Cryst.* B**40**, 300–306.
Thakkar, A. J., Koga, T., Saito, M. & Hoffmeyer, R. E. (1993). *Int. J. Quantum Chem. Symp.* **27**, 343–354.
Thomas, M. W. & Ghosh, R. E. (2012). *Mol. Phys.* **29**, 1489–1506.
Trueblood, K. N. & Dunitz, J. D. (1983). *Acta Cryst.* B**39**, 120–133.
Ugliengo, P., Pascale, F., Mérawa, M., Labéguerie, P., Tosoni, S. & Dovesi, R. (2004). *J. Phys. Chem. B*, **108**, 13632–13637.
Vosko, S. H., Wilk, L. & Nusair, M. (1980). *Can. J. Phys.* **58**, 1200.
Whitten, A. E. & Spackman, M. A. (2006). *Acta Cryst.* B**62**, 875–888.
Willis, B. T. M. & Howard, J. A. K. (1975). *Acta Cryst.* A**31**, 514–520.